

Microcavity enhanced directional transmission through a subwavelength plasmonic slit

Ali Haddadpour^{1,2} and Georgios Veronis^{1,2,*}

¹*School of Electrical Engineering and Computer Science, Louisiana State University, Baton Rouge, Louisiana 70803, USA*

²*Center for Computation and Technology, Louisiana State University, Baton Rouge, Louisiana 70803, USA*

[*gveronis@lsu.edu](mailto:gveronis@lsu.edu)

Abstract: We show numerically that a compact structure, consisting of multiple optical microcavities at both the entrance and exit sides of a subwavelength plasmonic slit, can lead to greatly enhanced directional transmission through the slit. The microcavities can increase the reflectivity at both sides of the slit, and therefore the resonant transmission enhancement. In addition, the microcavities can greatly improve the impedance matching, and therefore the coupling between free-space waves and the slit mode. An optimized structure with two microcavities on both the entrance and exit sides of the slit leads to ~ 16 times larger transmission cross section per unit angle in the normal direction compared to the optimized reference slit without microcavities. We also show numerically that the operation frequency range for high emission in the normal direction is broad.

© 2015 Optical Society of America

OCIS codes: (240.6680) Surface plasmons; (260.3910) Metal optics.

References and links

1. C. Genet and T. W. Ebbesen, "Light in tiny holes," *Nature* **445**, 39-46 (2007).
2. Z. Yu, G. Veronis, S. Fan, and M. L. Brongersma, "Design of mid-infrared photodetectors enhanced by surface plasmons on grating structures," *Appl. Phys. Lett.* **89**, 151116 (2006).
3. J. S. White, G. Veronis, Z. Yu, E. S. Barnard, A. Chandran, S. Fan, and M. L. Brongersma, "Extraordinary optical absorption through subwavelength slits," *Opt. Lett.* **34**, 686-688 (2009).
4. L. Verslegers, Z. Yu, P. B. Catrysse, and S. Fan, "Temporal coupled-mode theory for resonant apertures," *J. Opt. Soc. Am. B* **27**, 1947-1956 (2010).
5. H. J. Lezec, A. Degiron, E. Devaux, R. A. Linke, L. Martin-Moreno, F. J. Garcia-Vidal, and T. W. Ebbesen, "Beaming light from a subwavelength aperture," *Science* **297**, 820-822 (2002).
6. L. Martin-Moreno, F. J. Garcia-Vidal, H. J. Lezec, A. Degiron, and T. W. Ebbesen, "Theory of highly directional emission from a single subwavelength aperture surrounded by surface corrugations," *Phys. Rev. Lett.* **90**, 167401 (2003).
7. F. Lopez-Tejeira, S. G. Rodrigo, L. Martin-Moreno, F. J. Garcia-Vidal, E. Devaux, T. W. Ebbesen, J. R. Krenn, I. P. Radko, S. I. Bozhevolnyi, M. U. Gonzalez, J.-C. Weeber, and A. Dereux, "Efficient unidirectional nanoslit couplers for surface plasmons," *Nat. Phys.* **3**, 324-328 (2007).
8. T. Ishi, J. Fujikata, K. Makita, T. Baba, and K. Ohashi, "Si nano-photodiode with a surface plasmon antenna," *Jpn. J. Appl. Phys.* **44**, L364-L366 (2005).
9. W. Cai, J. S. White, and M. L. Brongersma, "Compact, high-speed and power-efficient electrooptic plasmonic modulators," *Nano Lett.* **9**, 4403-4411 (2009).
10. G. Gbur, H. F. Schouten, and T. D. Visser, "Achieving superresolution in near-field optical data readout systems using surface plasmons," *Appl. Phys. Lett.* **87**, 191109 (2005).

11. J. Fujikata, T. Ishi, H. Yokota, K. Kato, M. Yanagisawa, M. Nakada, K. Ishihara, K. Ohashi, T. Thio, and R. A. Linke, "Surface plasmon enhancement effect and its application to near-field optical recording," *Trans. Magn. Soc. Jpn* **4**, 255-259 (2004).
12. S. Shinada, J. Hashizume, and F. Koyama, "Surface plasmon resonance on microaperture vertical-cavity surface emitting laser with metal grating," *Appl. Phys. Lett.* **83**, 836-838 (2003).
13. B. Guo, G. Song, and L. Chen, "Plasmonic very-small-aperture lasers," *Appl. Phys. Lett.* **91**, 021103 (2007).
14. J. M. Yi, A. Cuche, E. Devaux, C. Genet, and T. W. Ebbesen, "Beaming visible light with a plasmonic aperture antenna," *ACS Photonics* **1**, 365-370 (2014).
15. J. Qi, T. Kaiser, R. Peucker, T. Pertsch, F. Lederer, and C. Rockstuhl, "Highly resonant and directional optical nanoantennas," *J. Opt. Soc. Am. A* **31**, 388-393 (2014).
16. W. Wang, D. Zhao, Y. Chen, H. Gong, X. Chen, S. Dai, Y. Yang, Q. Li, and M. Qiu, "Grating-assisted enhanced optical transmission through a seamless gold film," *Opt. Express* **22**, 5416-5421 (2014).
17. P. Kuang, J. M. Park, G. Liu, Z. Ye, W. Leung, S. Chaudhary, D. Lynch, K. M. Ho, and K. Constant, "Metal-nanowall grating transparent electrodes: Achieving high optical transmittance at high incident angles with minimal diffraction," *Opt. Express* **21**, 2393-2401 (2013).
18. Y. Liang, W. Peng, R. Hu, and H. Zou, "Extraordinary optical transmission based on subwavelength metallic grating with ellipse walls," *Opt. Express* **21**, 6139-6152 (2013).
19. F. J. Garcia-Vidal, L. Martin-Moreno, H. J. Lezec, and T. W. Ebbesen, "Focusing light with a single subwavelength aperture flanked by surface corrugations," *Appl. Phys. Lett.* **83**, 4500-4502 (2003).
20. N. Yu, Q. Wang, and F. Capasso, "Beam engineering of quantum cascade lasers," *Laser & Photon. Rev.* **6**, 24-46 (2012).
21. Q. Min and R. Gordon, "Surface plasmon microcavity for resonant transmission through a slit in a gold film," *Opt. Express* **16**, 9708-9713 (2008).
22. P. Ginzburg and M. Orenstein, "Plasmonic transmission lines: from micro to nano scale with $\lambda/4$ impedance matching," *Opt. Express* **15**, 6762-6767 (2007).
23. C. Min, L. Yang, and G. Veronis, "Microcavity enhanced optical absorption in subwavelength slits," *Opt. Express* **19**, 26850-26858 (2011).
24. G. Veronis and S. Fan, "Overview of simulation techniques for plasmonic devices," in *Surface Plasmon Nanophotonics*, M. L. Brongersma and P. G. Kik, eds. (Springer, 2007), pp. 169-182.
25. E. D. Palik, *Handbook of Optical Constants of Solids* (Academic, 1985).
26. J. Jin, *The Finite Element Method in Electromagnetics* (Wiley, 2002).
27. A. Taflov and S. C. Hagness, *Computational Electrodynamics: The Finite-Difference Time-Domain Method*, 3rd ed., (Artech House, 2005).
28. S. E. Kocabas, G. Veronis, D. A. B. Miller, and S. Fan, "Transmission line and equivalent circuit models for plasmonic waveguide components," *IEEE J. Sel. Topics Quantum Electron.* **14**, 1462-1472 (2008).
29. C. A. Balanis, *Antenna Theory: Analysis and Design* (Wiley-Interscience, 2005).
30. Y. Huang, C. Min, and G. Veronis, "Compact slit-based couplers for metal-dielectric-metal plasmonic waveguides," *Opt. Express* **20**, 22233-22244 (2012).
31. G. Veronis and S. Fan, "Theoretical investigation of compact couplers between dielectric slab waveguides and two-dimensional metal-dielectric-metal plasmonic waveguides," *Opt. Express* **15**, 1211-1221 (2007).
32. Z. Yu, A. Raman, and S. Fan, "Fundamental limit of nanophotonic light trapping in solar cells," *Proc. Natl. Acad. Sci. U.S.A.* **107**, 17491-17496 (2010).
33. Z. Ruan and S. Fan, "Superscattering of light from subwavelength nanostructures," *Phys. Rev. Lett.* **105**, 013901 (2010).
34. K. X. Wang, Z. Yu, S. Sandhu, V. Liu, and S. Fan, "Condition for perfect antireflection by optical resonance at material interface," *Optica* **1**, 388-395 (2014).
35. K. Krishnakumar, "Micro-genetic algorithms for stationary and non-stationary function optimization," *Proc. SPIE* **1196**, 289-296 (1990).

1. Introduction

Resonant nanoscale metallic apertures can efficiently concentrate light into deep subwavelength regions, and therefore greatly enhance the optical transmission through the apertures [1] or the absorption in or below the apertures [2–4]. In addition, grating structures, consisting of periodic arrays of grooves patterned on the metal film surrounding the entrance of the aperture, can excite surface plasmons on the metal surface. The excitation of surface plasmons enhances the coupling of incident light into the aperture [1, 2, 5–13]. When a grating structure is also formed on the exit side of the aperture, the transmission of light through the aperture can be highly directional [5, 6, 14–19]. Such beaming of light from metallic nanoapertures can lead

to numerous applications which include enhancing the performance of near-field devices for microscopy and data storage, and reducing the beam divergence of light sources such as lasers [5, 20]. However, the period of such gratings on the entrance and exit sides of the aperture has to be equal to the surface plasmon wavelength, and several grating periods are required. Thus, when operating at optical frequencies, such structures need to be several microns long to lead to enhanced directional transmission through the aperture.

It was previously demonstrated that the use of a single microcavity at the entrance and exit sides of a subwavelength plasmonic slit, can enhance the transmission cross section of the slit [4, 21]. In addition, it was shown that a microcavity can greatly enhance the coupling efficiency between a metal-dielectric-metal (MDM) waveguide of wavelength-sized width and a MDM waveguide of subwavelength width [22]. It was also demonstrated that the use of multiple microcavities at the entrance and exit sides of a subwavelength slit filled with an absorbing material can greatly enhance the absorption cross section of the slit [23].

In this paper, we show numerically that a compact structure, consisting of multiple optical microcavities at both the entrance and exit sides of a subwavelength plasmonic slit, can lead to greatly enhanced directional transmission through the slit. Our reference structure is an optimized subwavelength slit without microcavities. We show that the presence of the microcavities at the entrance and exit sides of the slit can lead to significantly larger reflectivity at both sides of the slit, and therefore to larger resonant transmission enhancement. In addition, the microcavities at the entrance and exit sides of the slit can greatly improve the impedance matching, and therefore the coupling between free-space waves and the slit mode. Such structures enhance both the incoupling of normally incident light from free space into the slit mode, as well as the outcoupling of light from the slit mode to free-space radiation in the normal direction. An optimized structure with two microcavities on both the entrance and exit sides of the slit leads to ~ 16 times larger transmission cross section per unit angle in the normal direction compared to the optimized reference slit without microcavities. We also show numerically that, while all structures were optimized at a single wavelength, the operation frequency range for high emission in the normal direction is broad.

The remainder of the paper is organized as follows. In Section 2, we define the transmission cross section and the transmission cross section per unit angle of the slit, and employ single-mode scattering matrix theory to account for their behavior. The results obtained for the reference slit without microcavities, as well as for the microcavity enhanced structures are presented in Section 3. Finally, our conclusions are summarized in Section 4.

2. Transmission cross section and transmission cross section per unit angle

We consider a structure consisting of a single slit in a silver film with N microcavities at the entrance side, and M microcavities at the exit side of the slit [Fig. 1(a)]. We use silver for the metal film due to its relatively low material loss at near-infrared wavelengths. Other metals such as gold can also be used. The structures are compact with all microcavity dimensions limited to less than $1.6 \mu\text{m}$.

We use a two-dimensional finite-difference frequency-domain (FDFD) method [24] to calculate the transmission through the structures as well as their radiation pattern. This method allows us to directly use experimental data for the frequency-dependent dielectric constant of metals such as silver [25], including both the real and imaginary parts, with no approximation. We use perfectly matched layer (PML) absorbing boundary conditions at all boundaries of the simulation domain [26]. We also use the total-field-scattered-field formulation to simulate the response of the structure to incident plane waves from free space with the electric field in plane [27].

We consider *symmetric* structures having the same number of microcavities on the entrance

and exit sides of the slit ($N = M$), and the same microcavity dimensions ($w_{Ti} = w_{Bi}, d_{Ti} = d_{Bi}, i = 1, \dots, N$). This is due to the fact that the optimized structures which lead to maximum emission in the normal direction for a normally incident plane wave were found to be symmetric. In other words, a multiple microcavities structure, which is optimum for incoupling normally incident light from free space into the slit mode, is also optimum for outcoupling light from the slit mode to free-space radiation in the normal direction.

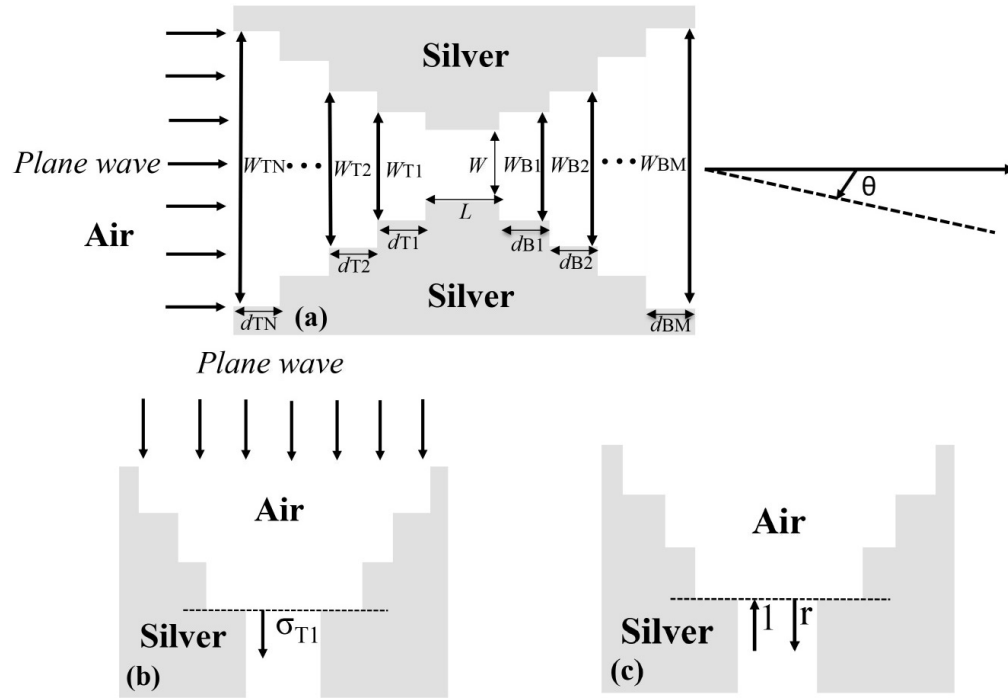


Fig. 1. (a) Schematic of a structure consisting of a slit in a silver film with N microcavities at the entrance side, and M microcavities at the exit side of the slit. (b) Schematic defining the transmission cross section σ_{T1} of a silver-air-silver waveguide through the structure above the entrance side of the slit of Fig. 1(a) for a normally incident plane wave from air. (c) Schematic defining the reflection r of the fundamental TM mode of a silver-air-silver waveguide at the interface of such a waveguide with the structures at the entrance and exit sides of the slit of Fig. 1(a).

For comparison of different configurations, we define the *transmission cross section* σ_T of the slit as the total power radiated from the slit (per unit length in two dimensions) normalized by the incident plane wave power flux. In two dimensions, the transmission cross section has units of length (m). We also define the *transmission cross section per unit angle* σ of the slit as the power radiated from the slit per unit angle normalized by the incident plane wave power flux. In two dimensions, the transmission cross section per unit angle has units of length per angle (m/rad).

We develop a single-mode scattering matrix theory to account for the behavior of these systems [28]. We define the transmission cross section σ_{T1} of a silver-air-silver MDM waveguide of width w (in the unit of length in two dimensions) as the transmitted power into the waveguide from the structure above the entrance side of the slit of Fig. 1(a), normalized by the incident plane wave power flux [Fig. 1(b)]. We also define r as the complex magnetic field reflection coefficient for the fundamental propagating TM mode in a silver-air-silver MDM waveguide

of width w at the interface of such a waveguide with the structures at the entrance and exit sides of the slit of Fig. 1(a) [Fig. 1(c)]. Finally, we define the directivity D as the ratio of the radiation intensity in a given direction from the slit to the radiation intensity averaged over all directions [29]. We use FDFD to numerically extract σ_{T1} and r [23, 28, 30]. We also use FDFD to numerically calculate the directivity $D(\theta)$ at an angle θ with respect to the normal as

$$D(\theta) = \frac{S_{PW}(\theta) \pi r_{FF}}{P_{out}}, \quad (1)$$

where $S_{PW}(\theta) = \frac{1}{2} \eta_0 |H_{FF}(\theta)|^2$ is the far-field power density at a distance r_{FF} above the slit, and at an angle θ with respect to the normal, and P_{out} is the total power emitted through the slit (per unit length in two dimensions). Here η_0 is the free-space impedance, and H_{FF} is the magnetic field in the far-field. We choose r_{FF} to be sufficiently far, so that the numerically calculated directivity becomes independent of r_{FF} [4]. The transmission cross section per unit angle of the slit at an angle θ with respect to the normal can then be calculated using scattering matrix theory as [23, 28, 30]:

$$\sigma(\theta) = \sigma_T \frac{D(\theta)}{\pi} = \sigma_{T1} \eta_{res} T \frac{D(\theta)}{\pi}, \quad (2)$$

where $T = 1 - |r|^2$ is the power transmission coefficient of the slit, $\eta_{res} = \left| \frac{\exp(-\gamma L)}{1 - r^2 \exp(-2\gamma L)} \right|^2$ is the resonance enhancement factor associated with the slit resonance, γ is the complex wave vector of the fundamental propagating TM mode in a silver-air-silver MDM waveguide of width w , and L is the length of the slit. Based on Eq. (1), we observe that, for fixed slit dimensions, w and L are fixed, so that the transmission cross section per unit angle of the slit σ is solely determined by σ_{T1} , r , and D . These three parameters in turn can be tuned by adjusting the geometrical dimensions of the microcavities at the entrance and exit sides of the slit.

3. Results

We first consider our reference structure consisting of a single subwavelength slit in a metal film [Fig. 2(a)]. In Fig. 2(b) we show the transmission cross section per unit angle in the normal direction $\sigma(\theta = 0^\circ)$ for such a structure as a function of the slit length L calculated using FDFD. The transmission cross section per unit angle is normalized with respect to w/π . A normalized transmission cross section per unit angle of one [$\sigma/(w/\pi) = 1$] therefore corresponds to a structure with transmission cross section equal to the geometric cross section of the slit ($\sigma_T = w$), which radiates isotropically in all directions [$D(\theta)=1$ for all θ]. We found that, as the slit length L increases, the transmission cross section per unit angle in the normal direction exhibits peaks, corresponding to the Fabry-Perot resonances in the slit. In Fig. 2(b) we also show the transmission cross section per unit angle in the normal direction calculated using scattering matrix theory [Eq. (2)]. We observe that there is excellent agreement between the scattering matrix theory and the exact results obtained using FDFD. Similarly, excellent agreement between the results of these two methods is observed for all the structures considered in this paper (Table 1). The maximum normalized transmission cross section per unit angle for the slit is ~ 7.25 [Fig. 2(b)]. For such a structure the transmission cross section σ_{T1} of the corresponding silver-air-silver MDM waveguide with width $w = 50$ nm is ~ 184 nm (Table 1), which is significantly larger than w . This is due to the fact that subwavelength MDM plasmonic waveguides collect light from an area significantly larger than their geometric cross-sectional area [31]. In addition, the resonance enhancement factor associated with the slit resonance is $\eta_{res} \sim 4.97$, and the maximum transmission cross section of the slit is $\sigma_T \sim 382$ nm (Table 1).

The properties of resonant apertures, such as the subwavelength slit in a metal film that we consider here, can be described using temporal coupled-mode theory [4]. Coupled-mode theory describes the interaction between a resonator and the surrounding environment using channels that couple to the resonance [32–34]. For the slit resonator one type of channel consists of free space plane waves propagating in different directions above and below the film [4]. If the metal is plasmonic, there are additional channels which consist of plasmonic modes at the top and bottom metal film surfaces [4]. The theory also includes loss channels associated with material absorption [4]. Based on temporal coupled-mode theory, the maximum transmission cross section for a subwavelength slit in a perfect electrical conductor (PEC) film is λ_0/π [4], which for $\lambda_0 = 1.55 \mu\text{m}$ gives $\lambda_0/\pi \sim 493 \text{ nm}$. As expected, the maximum transmission cross section of the slit in a plasmonic metal ($\sigma_T \sim 382 \text{ nm}$) is smaller than the maximum transmission cross section of a similar slit in a PEC film due to the material losses in the plasmonic metal [4].

In Fig. 3(a), we show the profile of the magnetic field amplitude for the structure of Fig. 3(a), normalized with respect to the field amplitude of the incident plane wave. The profile is shown for a slit length of $L=474 \text{ nm}$, which results in maximum transmission cross section per unit angle in the normal direction. We observe that, as expected for a subwavelength slit in a metallic film, the radiation pattern is almost isotropic [4]. The calculated directivity in the normal direction is $D(\theta = 0^\circ) \sim 0.969$ (Table 1). The directivity is smaller than one due to the presence of surface plasmon modes at the top surface of the metal film [4]. A portion of the light power exiting the slit couples to these plasmonic modes. The calculated directivity of the structure D as a function of the angle θ with respect to the normal is shown in Fig. 4.

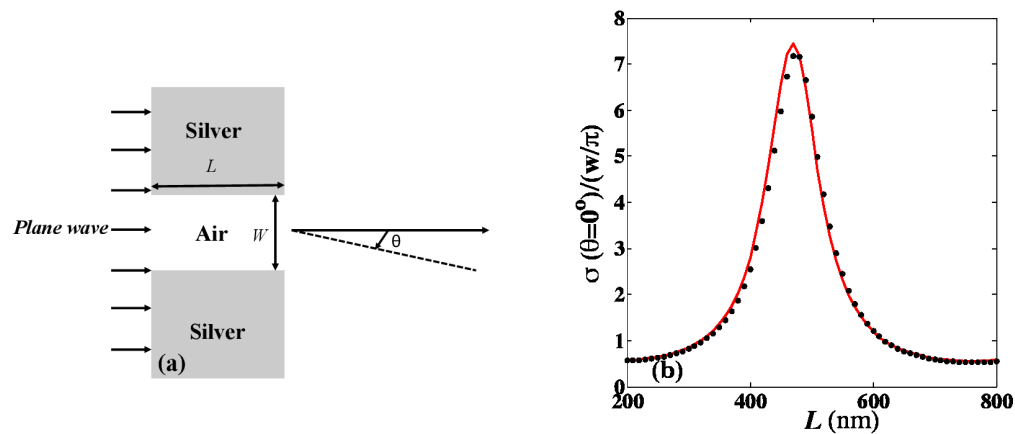


Fig. 2. (a) Schematic of a structure consisting of a single slit in a silver film. (b) Normalized transmission cross section per unit angle σ in the normal direction ($\theta = 0^\circ$) for the structure of Fig. 2(a) as a function of slit length L calculated using FDFD (black dots) and scattering matrix theory (red solid line). Results are shown for $w=50 \text{ nm}$ and $\lambda_0=1.55 \mu\text{m}$.

We next consider a structure with a single microcavity at each of the entrance and exit sides of the slit [Fig. 1(a) with $N = M = 1$]. With such a structure we aim to increase both the transmission of light through the slit as well as the directivity in the normal direction [4]. We use a genetic global optimization algorithm in combination with FDFD [23, 31, 35] to optimize the width and length of the two microcavities in the structure for maximum transmission cross section per unit angle in the normal direction $\sigma(\theta = 0^\circ)$. All structures are optimized at a single wavelength of $\lambda_0=1.55 \mu\text{m}$. However the structures can be designed to operate at other wave-

lengths in the near-infrared and visible. As mentioned above, all microcavity dimensions are limited to less than $1.6 \mu\text{m}$, and we consider symmetric structures. The maximum normalized transmission cross section per unit angle in the normal direction for such a structure is found to be ~ 33.5 (Table 1). For such a structure the transmission cross section σ_{T1} of the corresponding silver-air-silver MDM waveguide is $\sigma_{T1} \sim 169 \text{ nm}$ (Table 1), which is slightly smaller than the cross section for a slit without microcavities ($\sigma_{T1} \sim 184 \text{ nm}$). Thus, for the optimized ($N = 1, M = 1$) structure the presence of the microcavity at the entrance side of the slit does not severely affect the coupling of the incident light into the slit mode. However, the presence of the microcavities at the entrance and exit sides of the slit results in significantly larger reflectivity $|r|^2$ at the sides of the slit compared to a slit without microcavities (Table 1). Thus, the resonance enhancement factor for the optimized ($N = 1, M = 1$) structure is ~ 24.8 which is ~ 5 times larger than the one of the optimized reference slit without microcavities. In addition, the increased reflectivity at the sides of the slit leads to decrease of the power radiated from the slit. Thus, the power transmission coefficient of the slit for the optimized ($N = 1, M = 1$) structure is ~ 2.6 times smaller than the one of the optimized reference slit without microcavities. Overall, the use of an optimized single microcavity at the entrance and exit sides of the slit results in a slit transmission cross section $\sigma_T \sim 671 \text{ nm}$ (Table 1), which is ~ 1.8 times larger than the transmission cross section of the optimized slit without microcavities.

In Fig. 3(b), we show the profile of the magnetic field amplitude for the optimized ($N = 1, M = 1$) structure, normalized with respect to the field amplitude of the incident plane wave. We observe that for such a structure the directivity in the normal direction is increased compared to the slit without microcavities [Fig. 3(a)], and the radiation pattern is anisotropic. The calculated directivity in the normal direction is $D(\theta = 0^\circ) \sim 2.51$ (Table 1), which is ~ 2.6 times larger than the one of the optimized slit without microcavities. Overall, such a structure, when optimized, results in $1.8 \times 2.6 \sim 4.7$ times larger transmission cross section per unit angle in the normal direction compared to the optimized reference slit without microcavities [Fig. 2(a)]. The calculated directivity of the optimized ($N = 1, M = 1$) structure D as a function of the angle θ with respect to the normal is shown in Fig. 4.

We note that the ($N = 1, M = 1$) structure can be considered as a system of three coupled resonators (the slit and the two microcavities at the entrance and exit sides of the slit). These are also coupled to free space propagating plane waves above and below the structure as well as to plasmonic modes at the top and bottom metal film surfaces. The two microcavities are MDM waveguide resonators of width $w_{T1} = w_{B1}$ and length $d_{T1} = d_{B1}$. Due to the symmetry of the structure, normally incident plane waves can only excite even MDM modes in the microcavities. In addition, since the width of the optimized microcavities is smaller than the wavelength, only the fundamental MDM mode is propagating in the microcavities [28]. Since the width of the slit is much smaller than the width of the microcavities, the required length of the microcavities can be roughly estimated if the effect of the slit is ignored. Then each microcavity can be considered as a plasmonic transmission line resonator which is short-circuited on one side and open-circuited on the other [28]. Thus, the sum of the phases of the reflection coefficients at the two boundaries of the resonator is π . If we consider the Fabry-Perot resonance condition for the microcavities, we therefore find that the first resonant length of the microcavities is $\lambda_0/4$, which for $\lambda_0 = 1.55 \mu\text{m}$ gives $\lambda_0/4 \sim 388 \text{ nm}$. This rough estimate is close to the calculated optimized microcavity length $d_{T1} = d_{B1} = 430 \text{ nm}$ [Fig. 3(b)].

To further enhance the transmission cross section per unit angle of the slit in the normal direction, we consider a structure with multiple microcavities at both the entrance and exit sides of the slit [Fig. 1(a)]. More specifically, we use the genetic optimization algorithm in combination with FDFD to optimize the widths and lengths of the microcavities in a ($N = 2, M = 2$) structure for maximum transmission cross section per unit angle in the normal direction $\sigma(\theta = 0^\circ)$.

Table 1. Transmission cross sections σ_{T1} and σ_T , reflection coefficient r , resonance enhancement factor η_{res} , power transmission coefficient T , directivity in the normal direction $D(\theta = 0^\circ)$, and normalized transmission cross section per unit angle in the normal direction $\sigma(\theta = 0^\circ)/(w/\pi)$ calculated using scattering matrix theory and FDFD. Results are shown for the optimized structures of Fig. 1(a) with $(N, M) = (0, 0), (1, 1), (2, 2)$.

	(0,0)	(1,1)	(2,2)
σ_{T1}	184 nm	169 nm	645 nm
r	$0.763 \exp(2.56i)$	$0.916 \exp(2.62i)$	$0.786 \exp(2.62i)$
η_{res}	4.97	24.8	5.81
T	0.418	0.160	0.382
σ_T	382 nm	671 nm	1432 nm
$D(\theta = 0^\circ)$	0.969	2.51	4.00
$\sigma(\theta = 0^\circ)/(w/\pi)$ S-Matrix	7.40	33.7	115
$\sigma(\theta = 0^\circ)/(w/\pi)$ FDFD	7.25	33.5	113

As before, the dimensions of the structures at both the entrance and exit sides of the slit are limited to less than $1.6 \mu\text{m}$, and we consider symmetric structures. The maximum normalized transmission cross section per unit angle in the normal direction is found to be ~ 113 (Table 1). For such a structure the transmission cross section σ_{T1} of the corresponding silver-air-silver MDM waveguide is $\sigma_{T1} \sim 645 \text{ nm}$ (Table 1), which is ~ 3.5 larger than the cross section for a slit without microcavities ($\sigma_{T1} \sim 184 \text{ nm}$). Thus, for the optimized $(N = 2, M = 2)$ structure the microcavities at the entrance side of the slit greatly enhance the coupling between free space waves and the slit mode. This is consistent with previous findings that optimized multisection structures can greatly improve the impedance matching and therefore the coupling between optical modes [23, 31]. In addition, for the optimized $(N = 2, M = 2)$ structure the reflectivity $|r|^2$ at the sides of the slit is only slightly larger than the one of a slit without microcavities (Table 1). Thus, the resonance enhancement factor η_{res} for the optimized $(N = 2, M = 2)$ structure is only slightly increased with respect to the optimized reference slit without microcavities (Table 1). Overall, the use of two optimized microcavities at the entrance and exit sides of the slit results in a slit transmission cross section $\sigma_{T1} \sim 1432 \text{ nm}$ (Table 1), which is ~ 3.7 times larger than the transmission cross section of the optimized slit without microcavities. In addition, unlike the optimized single-microcavity structure in which the increased transmission is associated with increased resonance enhancement in the slit, for the optimized double-microcavity structure the increased transmission is mostly associated with improved impedance matching between free space waves and the slit mode.

In Fig. 3(c), we show the profile of the magnetic field amplitude for the optimized $(N = 2, M = 2)$ structure, normalized with respect to the field amplitude of the incident plane wave. We observe that for such a structure the directivity in the normal direction is further increased compared to the optimized slit without microcavities [Fig. 3(a)], and single-microcavity structure [Fig. 3(b)]. The calculated directivity in the normal direction is $D(\theta = 0^\circ) \sim 4$ (Table 1), which is ~ 4.1 times larger than the one of the optimized reference slit without microcavities. Overall, the double-microcavity structure, when optimized, results in $3.7 \times 4.1 \sim 16$ times larger transmission cross section per unit angle in the normal direction compared to the optimized reference slit without microcavities [Fig. 2(a)]. The calculated directivity of the optimized $(N = 2, M = 2)$ structure D as a function of the angle θ with respect to the normal is shown in Fig. 4. We observe that the radiation pattern of the optimized double-cavity structure is more anisotropic than the one of the optimized single-cavity structure.

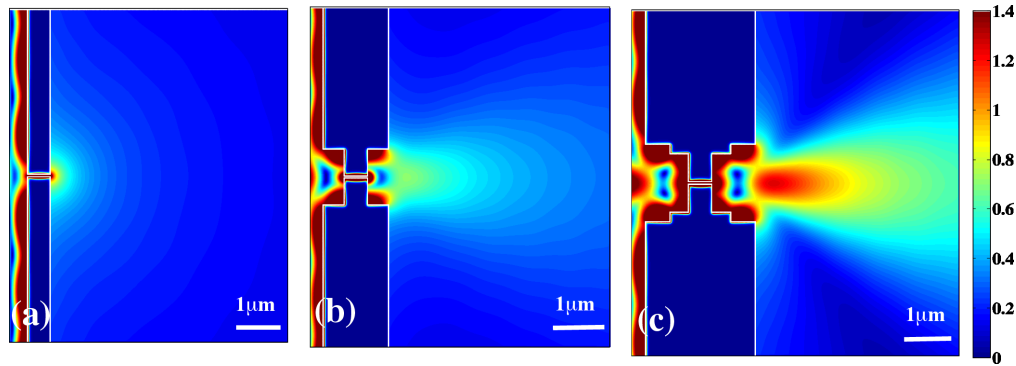


Fig. 3. (a) Profile of the magnetic field amplitude for the structure of Fig. 2(a), normalized with respect to the field amplitude of the incident plane wave. Results are shown for $L=474$ nm. All other parameters are as in Fig. 2(b). (b) Profile of the magnetic field amplitude for the structure of Fig. 1(a), normalized with respect to the field amplitude of the incident plane wave. Results are shown for $N=1, M=1$, and optimized parameters of $(w_{T1}, d_{T1}, w_{B1}, d_{B1}) = (1140, 430, 1140, 430)$ nm. All other parameters are as in Fig. 3(a). (c) Profile of the magnetic field amplitude for the structure of Fig. 1(a), normalized with respect to the field amplitude of the incident plane wave. Results are shown for $N=2, M=2$, and optimized parameters of $(w_{T1}, d_{T1}, w_{T2}, d_{T2}, w_{B1}, d_{B1}, w_{B2}, d_{B2}) = (1560, 500, 1200, 380, 1200, 380, 1560, 500)$ nm. All other parameters are as in Fig. 3(a).

All structures were optimized for maximum transmission cross section per unit angle in the normal direction at a single wavelength of $\lambda_0=1.55 \mu\text{m}$. In Fig. 5, we show the normalized transmission cross section per unit angle in the normal direction as a function of frequency for the optimized slit without microcavities [Fig. 3(a)], single-microcavity [Fig. 3(b)], and double-microcavity [Fig. 3(c)] structures. We observe that in all cases the operation frequency range for high emission in the normal direction is broad. This is due to the fact that in all cases the enhanced emission in the normal direction is not associated with any strong resonances. In other words, the quality factors Q of the microcavity structures are relatively low. The full width at half maximum for the optimized double-microcavity structure is larger than the one of the optimized single-microcavity structure. This is due to the fact that, as mentioned above, for the optimized single-microcavity structure the increased transmission is associated with a stronger slit resonance, while for the optimized double-microcavity structure the increased transmission is mostly associated with improved impedance matching. In Fig. 5 we also show the transmission cross section per unit angle in the normal direction for the optimized double-microcavity structure, if the metal in the structure is assumed to be lossless [$\epsilon_{\text{metal}} = \text{Re}(\epsilon_{\text{metal}})$], neglecting the imaginary part of the dielectric permittivity $\text{Im}(\epsilon_{\text{metal}})$]. As expected, in the presence of loss, the transmission through the structure decreases. However, this decrease is relatively small due to the compact wavelength-scale size of the structures.

4. Conclusions

In this paper, we numerically investigated compact structures, consisting of multiple optical microcavities at both the entrance and exit sides of a subwavelength plasmonic slit, with the goal to enhance the directional transmission through the slit. Our reference structure consisted of a subwavelength slit in a metal film without microcavities. We found that for such a structure, as the slit length increases, the transmission cross section per unit angle in the normal direction exhibits peaks, corresponding to the Fabry-Perot resonances in the slit. As expected

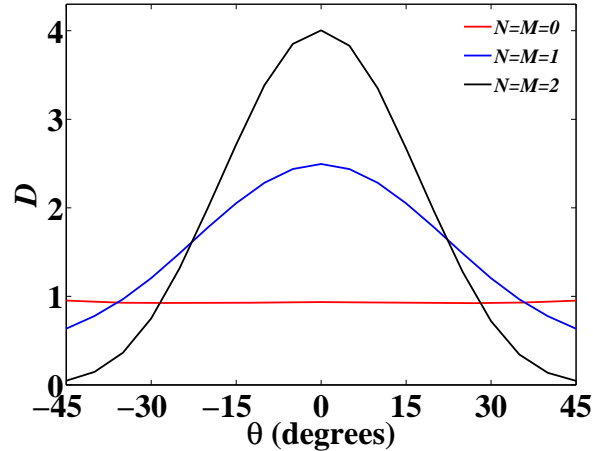


Fig. 4. Directivity D as a function of the angle θ with respect to the normal for the optimized structures of Fig. 1(a) with $N=M=0$ (red line), $N=M=1$ (blue line), and $N=M=2$ (black line). All other parameters for the $N=M=0$, $N=M=1$, and $N=M=2$ cases are as in Figs. 3(a), 3(b), and 3(c), respectively.

for a subwavelength slit in a metallic film, the radiation pattern is almost isotropic.

To enhance the directional transmission through the slit, we first considered a structure with a single microcavity at each of the entrance and exit sides of the slit. With such a structure we aimed to increase both the transmission of light through the slit, as well as the directivity in the normal direction. We found that the presence of the microcavities results in significantly larger reflectivity at the sides of the slit compared to a slit without microcavities. Thus, the resonance enhancement factor is greatly increased compared to the reference slit without microcavities. On the other hand, the increased reflectivity at the sides of the slit leads to decrease of the power radiated from the slit. Overall, the use of an optimized single microcavity at the entrance and exit sides of the slit results in a slit transmission cross section which is ~ 1.8 times larger than the transmission cross section of the optimized slit without microcavities. We also found that for such a structure the radiation pattern is anisotropic, and the directivity in the normal direction is ~ 2.6 times larger than the one of the optimized slit without microcavities. Overall, such a structure, when optimized, results in $1.8 \times 2.6 \sim 4.7$ times larger transmission cross section per unit angle in the normal direction compared to the optimized reference slit without microcavities.

To further enhance the transmission cross section per unit angle of the slit in the normal direction, we considered a structure with multiple microcavities at both the entrance and exit sides of the slit. We found that, unlike the optimized single-microcavity structure in which the increased transmission is associated with increased resonance enhancement in the slit, for an optimized double-microcavity structure the increased transmission is mostly associated with improved impedance matching between free-space waves and the slit mode. Such a structure enhances both the incoupling of normally incident light from free space into the slit mode, as well as the outcoupling of light from the slit mode to free-space radiation in the normal direction. The use of two optimized microcavities at the entrance and exit sides of the slit results in a slit transmission cross section which is ~ 3.7 times larger than the transmission cross section of the optimized slit without microcavities. We also found that for such a structure the

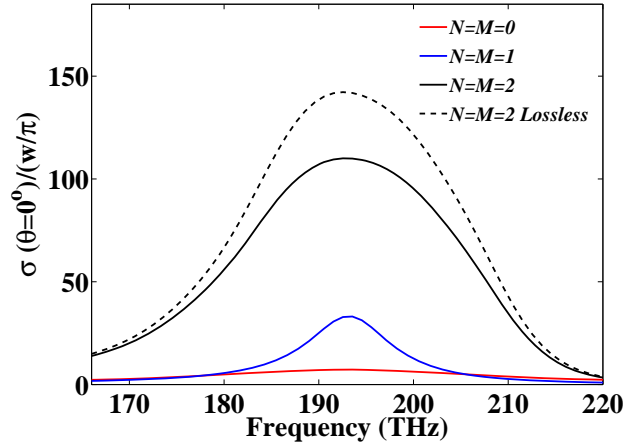


Fig. 5. Normalized transmission cross section per unit angle σ in the normal direction ($\theta = 0^\circ$) as a function of frequency for the optimized structures of Fig. 1(a) with $N=M=0$ (red line), $N=M=1$ (blue line), and $N=M=2$ (black line). All other parameters for the $N=M=0$, $N=M=1$, and $N=M=2$ cases are as in Figs. 3(a), 3(b), and 3(c), respectively. Also shown is the transmission cross section per unit angle in the normal direction for the optimized $N = M = 2$ structure, if the metal in the structure is assumed to be lossless (black dashed line).

directivity in the normal direction is ~ 4.1 times larger than the one of the optimized reference slit without microcavities. Overall, the double-microcavity structure, when optimized, results in $3.7 \times 4.1 \sim 16$ times larger transmission cross section per unit angle in the normal direction compared to the optimized reference slit without microcavities. We also found that, while all structures were optimized at a single wavelength, the operation frequency range for high emission in the normal direction is broad.

Acknowledgments

This research was supported by the Louisiana Board of Regents (contract LEQSF-EPS(2014)-PFUND-358), and the National Science Foundation (Awards No. 1102301 and 1254934).